Monthly Notices
of the
ROYAL ASTRONOMICAL SOCIETY

MNRAS **483,** 5687–5693 (2019) doi:10.1093/mnras/sty3441

# Multitude of iron lines including a Compton-scattered component in OAO 1657 – 415 detected with *Chandra*

Pragati Pradhan,[1,2]★ Gayathri Raman[3] and Biswajit Paul[3]

[1] *Penn State University, State College, PA 16801, USA*
[2] *St Joseph's College, Singamari, Darjeeling 734104, West Bengal, India*
[3] *Raman Research Institute, Sadashivnagar, Bangalore 560080, India*

Accepted 2018 December 14. Received 2018 December 14; in original form 2017 November 14

## ABSTRACT

We present a high-resolution X-ray spectrum of the accreting X-ray pulsar OAO 1657 – 415 obtained with HETG + ACIS-S onboard *Chandra*, revealing the presence of a broad line component around ∼6.3 keV associated with the neutral iron $K_\alpha$ line at 6.4 keV. This is interpreted as a Compton shoulder arising from the Compton-scattering of the 6.4-keV fluorescence photons, making OAO 1657–415 the second accreting neutron star in which such a feature has been detected. A Compton shoulder reveals the presence of dense matter surrounding the X-ray source. We did not detect any periodicity in the light-curve and we obtained an upper limit of ∼2 per cent for the pulse fraction during this observation. This could be a result of the smearing of the pulses when X-ray photons are scattered from a large region around the neutron star. In addition to the Fe $K_\alpha$, Fe $K_\beta$ and Ni $K_\alpha$ lines already reported for this source, we report for the first time the presence of He-like and H-like iron emission lines at 6.7 and 6.97 keV in the first-order HETG spectrum. The detection of such ionized lines, indicative of a highly ionized surrounding medium, is rare in X-ray binaries.

**Key words:** stars: pulsars: general – X-rays: binaries – X-rays: individual: OAO 1657 – 415.

## 1 INTRODUCTION

The X-ray spectrum of an accreting neutron star in a high-mass X-ray binary (HMXB) can in most cases be described by a power law with a photon index in the range of 0.5–1.5 and a high-energy cut-off typically at 10–20 keV, along with a cyclotron resonance scattering feature (CRSF) and an iron $K_\alpha$ emission line at 6.4 keV. A few HMXBs with low absorption column densities also often show a soft excess (see e.g. Paul et al. 2002). The iron emission lines, produced by fluorescence emission, play a significant role in probing the matter surrounding the neutron star. In addition, at very large values of the ionization parameter, we see He-like and H-like iron emission lines at 6.7 and 6.97 keV. Some of these ionized lines are seen in a few X-ray binaries, such as Cen X–3 (Wojdowski et al. 2004; Iaria et al. 2005; Naik, Paul & Ali 2011) and Cyg X–3 (Paerels et al. 2000). If the Compton optical depth of the medium is high (>0.1; Watanabe et al. 2003), then this emitted photon of energy at 6.4 keV can be further Compton-scattered in the same medium and lose some energy (around 156 eV for back-scattered photons; Watanabe et al. 2003). Such scattered photons produce a shoulder at a lower energy, termed the Compton shoulder.

Thanks to the unmatched spectral resolution of *Chandra*, the first-order Compton shoulder has already been observed in one HMXB, namely GX 301–2 (Watanabe et al. 2003). Another source with a high absorption and strong iron line similar to in GX 301–2 is OAO 1657 – 415. OAO 1657 – 415 is an eclipsing X-ray binary discovered with the *Copernicus* satellite (Polidan et al. 1978), with the companion star being a type Ofpe/WN9 supergiant (Mason et al. 2009) and the neutron star having a pulse period of ∼38 s (White & Pravdo 1979). A study of the dust-scattered halo with *ASCA* estimated the distance to the source as 7.1 ± 1.3 kpc (Audley et al. 2006), in agreement with the earlier estimated distance of 6.4 ± 1.5 kpc obtained from the study of the infrared counterpart (Chakrabarty et al. 2002). The orbital period of this system is ∼10.5 d (Chakrabarty et al. 1993), with an orbital decay rate of $\dot{P}_{\rm orb} \sim (-9.74 \pm 0.78) \times 10^{-8}$ (Jenke et al. 2012), and the eccentricity of the orbit is ∼0.1 (Chakrabarty et al. 1993; Bildsten et al. 1997; Jenke et al. 2012). The X-ray light-curves of OAO 1657 – 415 show a large variation in intensity even outside the eclipse (Barnstedt et al. 2008). The same authors (Barnstedt et al. 2008) also noted the presence of an unexplained (possibly temporary) dip at phase ∼0.55 in the RXTE/All-Sky Monitor (ASM) light-curve of OAO 1657 – 415. In the broad-band X-ray spectra obtained with *BeppoSAX* and *Suzaku*, the possible existence of a CRSF at ∼36 keV was seen with limited statistical significance, indicating a magnetic field strength of $3.2(1 + z) \times 10^{12}$ G, where $z$ is the gravitational redshift (Orlandini et al.

★ E-mail: pragati2707@gmail.com

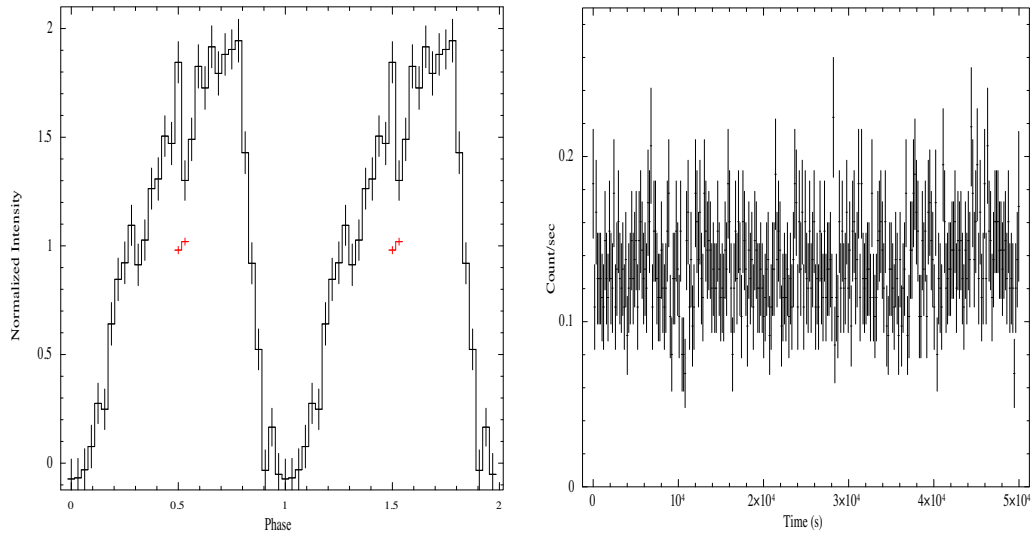


**Figure 1.** (Left) Orbital intensity profile of OAO 1657–415 with the RXTE/ASM and *Chandra*/ACIS-S light-curves folded at an orbital period of 10.44749 d (Falanga et al. 2015). Phase zero corresponds to the mid-eclipse time MJD 506 89.116 (Falanga et al. 2015). (Right) ACIS-S light-curve binned at ∼174 s. The zero of the light-curve is ∼ MJD 556 98.5781.

1999; Barnstedt et al. 2008; Pradhan et al. 2014). Detailed time-resolved spectroscopy of OAO 1657 – 415 with *Suzaku* showed a large variation in the absorption column density along with a very large equivalent width of the iron $K_\alpha$ line at some time intervals during a long observation (Pradhan et al. 2014). These changes indicate the neutron star passing through a dense clump, giving rise to a high column density, similar to the pre-periastron passage of GX 301–2 (Islam & Paul 2014). Such conditions are conducive for the formation of a Compton shoulder. This prompted us to examine the high-resolution *Chandra* spectrum of OAO 1657 – 415, where such a feature would be discernible.

## 2 OBSERVATION AND DATA ANALYSIS

OAO 1657 – 415 was observed with *Chandra* at the same phase (0.5–0.6) as where a transient dip had earlier been noticed in the ASM light-curves (Barnstedt et al. 2008). The observation was carried out from 2011 May 17, 13:29:11 UT until 2011 May 18, 03:48:54 UT with a high-energy transmission grating (HETG; Canizares et al. 2005) for 50 ks. The HETG consists of two transmission gratings: a medium-energy grating (MEG; 0.4–5.0 keV), and a high-energy grating (HEG; 0.8–10.0 keV). The dispersed grating spectra are recorded with an array of CCDs – the Advanced CCD Imaging Spectrometer (ACIS-S; Garmire et al. 2003). Data were reprocessed using the package *Chandra* Interactive Analysis of Observations (CIAO, version 4.8) following the Chandra X-ray Center (CXC) guidelines.[1] The evt1 files were reprocessed with `the` 'chandra_repro' script, which automates the recommended reprocessing steps and results in processed evt2 files ready for scientific analysis. This observation was made in 'Timed exposure' in half of the ACIS-S CCDs (512 rows), beginning with the first row of the CCD. To extract the ACIS-S light-curve, we used the command `'dmextract'` for CCD_ID = 7 in the evt2 files with the following region selection. The source region was chosen at the centre of the ACIS-S image with a radius of 5 arcsec, and the background region was chosen as an annulus with an inner (outer) radius of 7 (15) arcsec. The ACIS-S spectrum was also extracted with the same region selection and event file using the command `'specextract'`. For the light-curve extraction from HETG, we defined the source region as a box with length (breadth) 660 (10) arcsec, while excluding the zero-order central region (corresponding to the centre of the ACIS-S image). For the background region, we excluded this central ACIS-S source region along with the HETG source region and defined a region of the same size as the HETG source region. The background-corrected light-curve was then extracted with the command `'dmextract'`. The light-curves from both the instruments were barycentre-corrected using the orbit ephemeris file during the observation with the help of the command `'axbary'`. The spectral products for HEG for different orders are automatically obtained while executing the `'chandra_repro'` script. The same script also creates the response matrices for the respective grating orders. The positive and negative diffraction first-order spectra and their corresponding response files, so obtained, were added using `'combine_grating_spectra'`.[2] The resultant spectra for both instruments were grouped with a minimum of 20 counts per bin, and finally spectral fitting was carried out with `xspec` version 12.9.0.

## 3 RESULTS

### 3.1 Timing analysis

We folded the ACIS-S light-curves (Fig. 1, right) along with the RXTE/ASM light-curve at a period of 10.447 49 d (Falanga et al. 2015) to obtain the orbital profile of OAO 1657 – 415, as is shown in the left panel of Fig. 1. The observation was carried out during orbital phases ∼0.5–0.6, where phase zero corresponds to the mid-eclipse time MJD 506 89.116 (Falanga et al. 2015). In the right panel of the same figure, we have plotted the ACIS-S light-curve binned at 100 times the original binning at ∼174 s. We searched for

[1] http://cxc.harvard.edu/ciao/threads/

[2] The higher-order spectra are too faint for any meaningful analysis and are therefore not used.

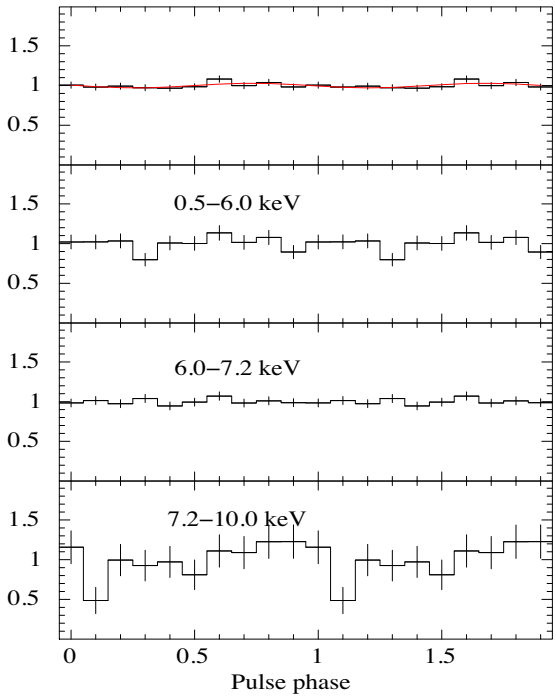


**Figure 2.** The uppermost panel represent the average ACIS-S light-curve folded at a spin period of 36.968 638 s estimated from the *Fermi* GBM history of the source during this epoch. The ACIS-S light-curve has been fitted with a sine wave (plus a constant) to determine the pulse fraction. The second, third and fourth panels are the energy-resolved ACIS-S light-curves folded at the same period. The lack of pulsations is clearly seen.

periodicity in both the ACIS-S and the HETG light-curves (binned at 1.74 s) using the FTOOLS task `'efsearch'` but did not detect any. We then investigated the pulse period evolution history of the source measured with the Fermi Gamma Ray Burst Monitor (GBM) and found the spin period of this pulsar during the time of this observation to be 36.968 638 s. The zeroth-order light-curve, which has more sensitivity and better statistics than the curve from the HETG, was then folded at this period, as shown in Fig. 2. The upper limit on the pulse fraction (Pmax – Pmin)/(Pmax + Pmin), where Pmax and Pmin correspond to the maximum and minimum pulse amplitude, respectively) for the ACIS-S light-curve was about 2 per cent. Note that we did not carry out any orbital correction when searching for periodicity. This is because the decoherence time-scale[3] for this system is nearly 1 d, which is much longer than this observation duration ($T$) of ∼50 ks, and the maximum smearing[4] of the pulse phase without an orbital motion correction ($\delta t_{max}$) is estimated to be about 1.6 s, which is only a small fraction of the pulsar spin period of ∼37 s. Furthermore, we also created the energy-resolved pulse profiles of OAO 1657 – 415 (Fig. 2) in the energy ranges of 0.5–6.0, 6.0–7.2 and 7.2–10.0 keV. We did not detect any pulsations in these light-curves either.

In order to verify this lack of pulsations in OAO 1657 – 415, an identical data-reduction and analysis procedure was carried out on the *Chandra* observations of a pulsar with comparable pulse period and brightness, namely XTE J1946 + 274. This object is a transient Be-HMXB pulsar with a spin period of nearly 15.8 s (Smith & Takeshima 1998). A 5-ks-long archival *Chandra* observation (Obs-ID 14646), which was carried out when this source was in quiescence, was analysed for this purpose. We processed the evt1 files using the CIAO script `'chandra_repro'` and obtained the evt2 files. We then extracted the ACIS-S zeroth-order light-curves using the tool `'dmextract'`. This light-curve binned at 174 s is shown in the left panel of Fig. 3. The FTOOL task `'efsearch'` was adopted to carry out a period search in the light-curve. The `'efsearch'` procedure folds the light-curve with a large number of trial periods around a specified approximate period, after which a constant is fitted to the folded light-curve and the resultant $\chi^2$ is obtained. The trial period that shows the maximum $\chi^2$ represents the true period. Using our light-curve of XTE J1946 + 274, we performed a narrow period search in the range 15.6 to 15.8 s with a step size of $1 \times 10^{-4}$ s. We found a peak in the $\chi^2$, which we fitted using a Gaussian, and determined the pulse period to be 15.758 ± 0.003 s. This period was then used to fold the light-curve (as shown in middle and right panels of Fig. 3), and we obtained a pulse fraction (defined as (Imax – Imin)/(Imax + Imin) of 0.67 ± 0.20. With the same data reduction and analysis methods as described above, we were able to reproduce the results of Özbey Arabacı et al. (2015). This re-affirms the fact that the *Chandra* data of OAO 1657 – 415 indeed lacks pulsations, possible reasons for which are suggested in Section 4.

### 3.2 Spectral analysis

The zero-order ACIS-S and the first-order HETG spectra (HEG 1) of OAO 1657 – 415 were fitted separately.[5] The X-ray spectrum is dominated by iron emission lines, with X-ray photons at 6.0–7.2 keV comprising ∼58 per cent of the total X-ray photons detected in the band 0.5–10.0 keV. For the ACIS-S continuum spectrum, we fitted a power law along with the line-of-sight photoelectric absorption and Compton scattering component (`'cabs'`) with solar abundances *angr* (Anders & Grevesse 1989). Three Gaussian lines (which are clearly seen in the raw spectrum) corresponding to the $K_\alpha$ and $K_\beta$ lines of iron and the $K_\alpha$ line of nickel at 7.4 keV were added to obtain a reduced $\chi^2$ ($\chi^2_{red}$) of 2.71, while the spectrum has 153 degrees of freedom (d.o.f). The addition of another Gaussian line at 6.7 keV (with its width frozen to the best-fit value) reduced the $\chi^2_{red}$ (d.o.f) to 2.05 (151). To correct for the wavy residuals, we introduced the partial covering absorption model, as is needed to describe the X-ray spectrum of OAO 1657 – 415 (Pradhan et al. 2014) for which the $\chi^2_{red}$ (d.o.f) is now 1.1 (149). Interestingly, we noticed that the residuals still show an asymmetry near the iron $K_\alpha$ line. To fit this, we added another Gaussian line centred at ∼6.3 keV, and a $\chi^2_{red}$ of 0.94 was obtained with 146 d.o.f. On further inspection, a better fit to the same asymmetry was obtained with a two-step function (convolved with Gaussian) in `xspec` such that one of the line energies is tied to the line energy of the iron $K_\alpha$ line, and the other is fixed at ($K_\alpha$ – 0.16 keV), with the widths of both as zero and their normalizations equal but opposite in sign. For this model, the $\chi^2_{red}$ obtained was 0.92 for 148 d.o.f. We chose the latter model to represent the additional broad low-energy component associated with the iron $K_\alpha$ line.

The HETG spectrum was fitted independently, with the same spectral model as the ACIS-S spectrum, with the difference that because the $K_\alpha$ line of nickel was outside the band used for HETG fitting, we did not detect it. Instead, we detected another line at 6.97 keV in the HETG spectrum, thanks to the better spectral

[3]Obtained from equation (A9) of Chakrabarty et al. (1997).
[4]$\delta t_{max} = ax \sin i(1 - \cos\theta)/c$, where $\theta = T/P_{orb} \times 2\pi$.

[5]Note that the ACIS-S (HEG 1) spectrum was 17 (15) per cent piled up

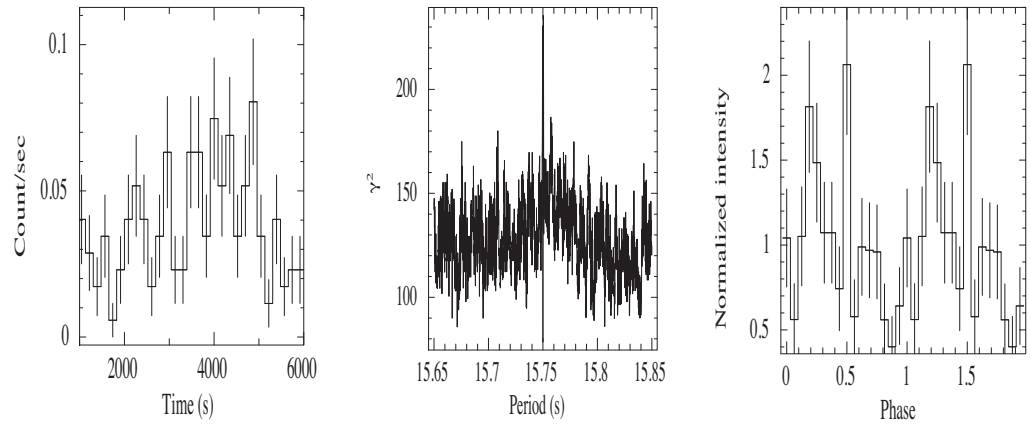


**Figure 3.** (Left) Background-subtracted light-curve of XTE 1946 + 274 binned at ∼174 s. (Middle) Period search with `'efsearch'`. (Right) Folded pulse profile of XTE 1946 + 274. The presence of pulsations obtained with the same analysis procedure as used for OAO 1657–415 ensures that the lack of pulsations in the latter is not a result of the data reduction procedure.

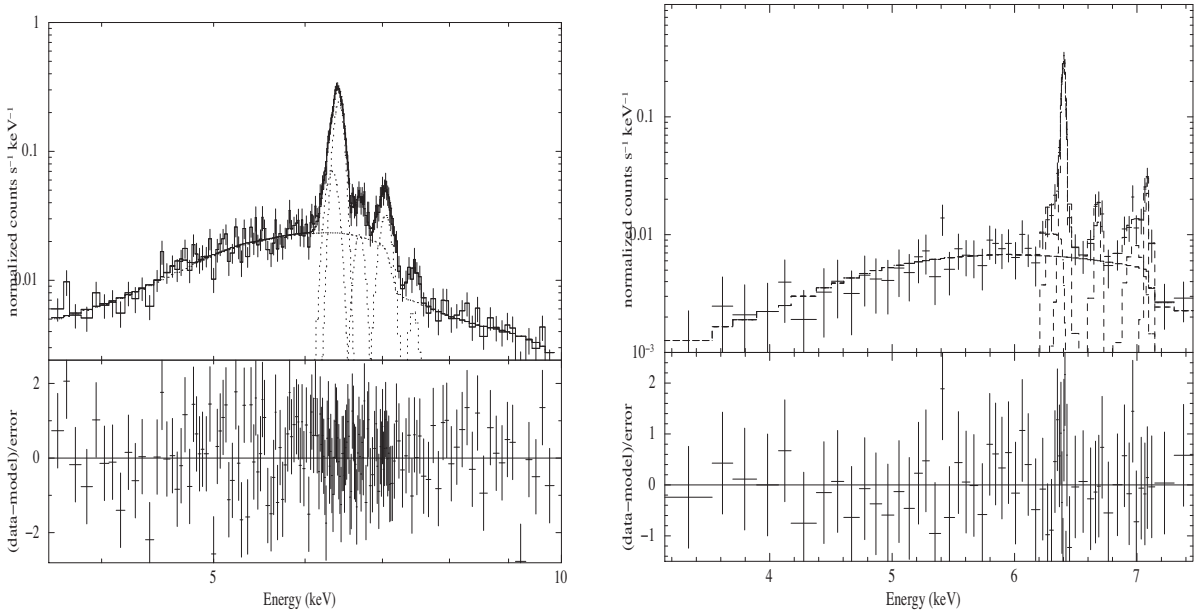


**Figure 4.** (Left) ACIS-S spectrum of OAO 1657 – 415 in the energy range of 3.5–10.0 keV with a two-step function that fits the Compton shoulder of the 6.4-keV line and emission lines at 6.4 (Fe $K_\alpha$), 6.7 (He-like iron), 7.1 (Fe $K_\beta$) and 7.4 (Ni $K_\alpha$) keV. (Right) HETG spectrum of OAO 1657 – 415 in the energy range of 3.0–7.5 keV with a two-step function that fits the Compton shoulder of the 6.4-keV line and emission lines at 6.4 (Fe $K_\alpha$), 6.7 (He-like iron), 6.97 (H-like iron) and 7.1 (Fe $K_\beta$) keV.

resolution of HETG compared with ACIS-S. The X-ray spectra of both the instruments are shown in Fig. 4, and the details of the spectral parameters – with and without using an additional component at ∼6.3 keV – are given in Table 1. The analytical form of the model is

$$\mathrm{S(E)} = \mathrm{e}^{-N_{\mathrm{H1}}\sigma(E)} \times (K\ E^{-\Gamma} \times (f\mathrm{e}^{-N_{\mathrm{H2}}\sigma(E)} + (1-f)) + 4\ \mathrm{Ga} + 2\ \mathrm{Step\ function}), \quad (1)$$

where $K$, $N_{\mathrm{H1}}$, $\sigma(E)$ and $\Gamma$ are the normalization (in units of photons keV$^{-1}$ cm$^{-2}$ s$^{-1}$ at 1 keV), the hydrogen column density (in units of $10^{22}$ atoms cm$^{-2}$), the photoelectric with Compton scattering cross-section, and the photon index, respectively, while $N_{\mathrm{H2}}$ is the partial covering column density (in units of $10^{22}$ atoms cm$^{-2}$) with the covering fraction as $f$. A plausible explanation for the additional component at ∼6.3 keV is the presence of a Compton shoulder.[6] The individual fits are shown in Fig. 4.

To demonstrate this, we remove the Compton shoulder line from the fit and plot the resultant spectrum in Fig. 5. The positive excess marked with the arrow is evidence of the need for an additional, fairly broad component at ∼6.3 keV, which is the Compton shoulder.

[6]We also cross-checked the presence of a Compton shoulder by taking into consideration the doublet structure of the $K_\alpha$ and $K_\beta$ lines of iron. For this, we fitted the $K_\alpha$ ($K_\beta$) line with two Gaussian lines, the energy of one less than that of the other by 13.2(16.0) eV and the relative normalizations in the ratio 2:1(2:1) as suggested in Barragán et al. (2009). The asymmetry in the $K_\alpha$ line is still evident in the X-ray spectrum, consistent with our fitting performed by using one Gaussian each for the $K_\alpha$ and $K_\beta$ lines.

**Table 1.** Best-fit phase-averaged spectral parameters of OAO 1657 – 415. Errors quoted are for the 90 per cent confidence range.

| Parameter | HETG | HETG without Compton shoulder | ACIS-S | ACIS-S without Compton shoulder |
|---|---|---|---|---|
| $N_{H1}{}^{a}$ | $8^{+6}_{-6}$ | $8^{+7}_{-6}$ | $10^{+4}_{-4}$ | $8^{+3}_{-2}$ |
| $N_{H2}{}^{a}$ | $48^{+5}_{-4}$ | $48^{+5}_{-4}$ | $66^{+3}_{-3}$ | $70^{+2}_{-2}$ |
| $f$ | $0.95^{+0.05}_{-0.02}$ | $0.95^{+0.04}_{-0.05}$ | $0.96^{+0.01}_{-0.01}$ | $0.96^{+0.01}_{-0.01}$ |
| $\Gamma$ | $0.21^{+0.08}_{-0.07}$ | $0.19^{+0.06}_{-0.05}$ | $0.27^{+0.14}_{-0.14}$ | $0.38^{+0.14}_{-0.14}$ |
| $\Gamma^{b}_{norm}$ | $0.0013 \pm 0.0001$ | $0.0011 \pm 0.0001$ | $0.0014^{+0.0004}_{-0.0003}$ | $0.0019 \pm 0.0004$ |
| Step line flux$^{c}$ | $8.8^{+1.7}_{-4.8}$ | - | $16.3^{+1.8}_{-1.8}$ | - |
| Line centre (keV) | $6.40 \pm 0.01$ | $6.40 \pm 0.01$ | $6.41 \pm 0.01$ | $6.39 \pm 0.01$ |
| Line width (keV) | $0.008 \pm 0.002$ | $0.009 \pm 0.002$ | $0.013^{+0.04}_{-0.03}$ | $0.041^{+0.005}_{-0.005}$ |
| Line norm$^{d}$ | $65.3 \pm 4.5$ | $68.0 \pm 4.4$ | $49.3^{+4.3}_{-5.9}$ | $63.8^{+2.6}_{-2.5}$ |
| EW (keV) | $1.12 \pm 0.07$ | $1.46 \pm 0.08$ | $0.79^{+0.07}_{-0.09}$ | $1.73^{+0.05}_{-0.05}$ |
| Line centre (keV) | $6.68^{+0.02}_{-0.01}$ | $6.68^{+0.02}_{-0.02}$ | $6.69^{+0.02}_{-0.02}$ | $6.69^{+0.02}_{-0.02}$ |
| Line width (keV) | 0.022 | $0.022 \pm 0.015$ | 0.025 | 0.001 |
| Line norm$^{d}$ | $6.6 \pm 2.8$ | $6.1 \pm 2.7$ | $5.8^{+1.1}_{-1.1}$ | $4.9^{+1.2}_{-1.1}$ |
| EW (keV) | $0.04 \pm 0.02$ | $0.04 \pm 0.01$ | $0.05 \pm 0.01$ | $0.04 \pm 0.01$ |
| Line centre (keV) | $6.97 \pm 0.03$ | $6.97 \pm 0.03$ | – | – |
| Line width (keV) | $0.068^{+0.045}_{-0.023}$ | $0.062^{+0.044}_{-0.037}$ | – | – |
| Line norm$^{d}$ | $11.3^{+4.4}_{-5.5}$ | $10.2^{+5.1}_{-4.6}$ | – | – |
| EW (keV) | $0.21 \pm 0.08$ | $0.18 \pm 0.09$ | – | – |
| Line centre (keV) | $7.08 \pm 0.01$ | $7.07 \pm 0.01$ | $7.05^{+0.01}_{-0.01}$ | $7.06^{+0.01}_{-0.01}$ |
| Line width (keV) | 0.0003 | 0.0003 | $0.06^{+0.02}_{-0.02}$ | $0.06^{+0.02}_{-0.02}$ |
| Line norm$^{d}$ | $9 \pm 3$ | $9.3 \pm 3.4$ | $14.2 \pm 1.8$ | $14.6 \pm 2.1$ |
| EW (keV) | $0.18 \pm 0.07$ | $0.20 \pm 0.07$ | $0.46 \pm 0.06$ | $0.46 \pm 0.06$ |
| Line centre (keV) | – | – | $7.45 \pm 0.04$ | $7.45 \pm 0.4$ |
| Line width (keV) | – | – | 0.04 | 0.04 |
| Line norm$^{d}$ | – | – | $3.0 \pm 1.5$ | $3.1 \pm 1.2$ |
| EW (keV) | – | – | $0.12 \pm 0.04$ | $0.12 \pm 0.04$ |
| $\chi^2_\nu$/d.o.f | 0.74/47 | 1.1/48 | 0.92/148 | 1.1/149 |
| Flux$^{e}$ (1-10 keV) | $2.99 \pm 0.12$ | $2.99 \pm 0.24$ | $2.41 \pm 0.05$ | $2.42 \pm 0.05$ |

*Notes.* $^{a}$In units of $10^{22}$ atoms cm$^{-2}$;
$^{b}$in units of photons keV$^{-1}$ cm$^{-2}$ s$^{-1}$ at 1 keV;
$^{c}$in units of photons cm$^{-2}$ s$^{-1}$ $\times 10^{-5}$ with a step line energy at 6.4 and (6.4–0.16) for the width of both fixed at zero;
$^{d}$in units of photons cm$^{-2}$ s$^{-1}$ $\times 10^{-5}$;
$^{e}$in units of $10^{-11}$ erg cm$^{-2}$ s$^{-1}$.

The Compton shoulder is detected in both the ACIS-S and HETG spectra independently, with a reduction in $\chi^2$ of 22 and 16 respectively for the addition of one component. The probability of chance improvement (PCI) using an F-test in `xspec` on the addition of the Compton shoulder in the ACIS (HETG) spectrum is $2.4 \times 10^{-6}$ ($2.9 \times 10^{-5}$). This low value of PCI also adds significance to the presence of a Compton shoulder.

## 4 DISCUSSION

Supergiant stars have strong stellar winds that are often inhomogenous, and the passage of the neutron star in an HMXB through clumps of varying size and wind density leads to variable accretion, column density and emission line strength. If the neutron star passes through a very dense clump of matter, the reprocessing of the source photons in the material will produce an iron fluorescence line, and a Compton shoulder will be produced if a large enough fraction of the $K_\alpha$ iron line photons are scattered by electrons in the dense medium surrounding the X-ray source. A careful analysis of the ACIS-S and HETG spectra of OAO 1657 – 415 has led to the detection of this Compton shoulder, along with a very high column density of absorption. The observation was carried out at $\sim$ phase 0.55 in the ASM light-curves (Fig. 1, left), a phase at which there have been reports of temporary dips (Barnstedt et al. 2008). A timing analysis of OAO 1657 – 415 allowed us to place an upper limit on the pulse fraction ($\sim$2 per cent; Fig. 2). The low pulse fraction is reminiscent of one part of a long *Suzaku* observation (segment C in Pradhan et al. 2014), which was interpreted as showing the source passing through a dense clump of matterduring which time, the pulse fraction was the lowest. During the same segment C, the equivalent width of the iron $K_\alpha$ line was also the strongest, which implies that the neutron star was passing *through* a clump (see section 4.1 of Pradhan et al. 2014 for details). These highly absorbed states seem to be present at multiple phases (segment C occurs around phase 0.25, and the current observation is at phase $\sim$0.55), indicating that the orbit of OAO 1657 – 415 has clumps of matter at different phases. In a luminous HMXB system, the wind near the neutron star is photoionized by X-rays from the neutron star (see e.g. Watanabe et al. 2006). During this *Chandra* observation, in addition to the iron $K_\alpha$ and $K_\beta$ lines, we also detected $K_\alpha$ emission from highly ionized ions: H-like Fe corresponding to 6.97 keV. Among the three He triplets at

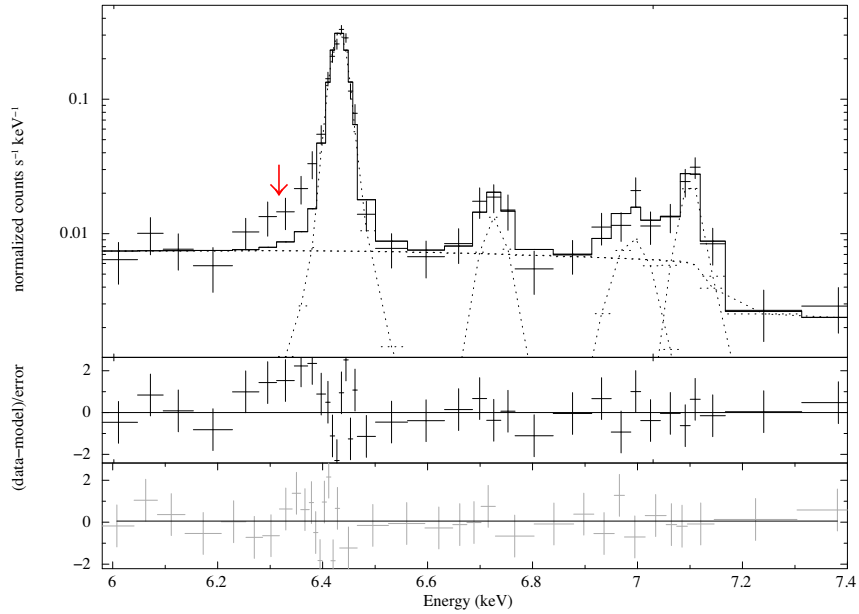


**Figure 5.** The HETG spectrum (6–7.4 keV) of OAO 1657 – 415 is shown in the top panel, along with the best-fit model without the two-step function for the Compton shoulder. The residual to this fit is shown in the middle panel, and the residual to the fit after inclusion of the two-step function is shown in the bottom panel.

6.63, 6.67 and 6.70 keV, we were able to resolve the emission line at 6.70 keV. In addition to this, $K_\alpha$ lines of nickel are also seen.

So far, a Compton shoulder has been reported in the X-ray specrum of only one X-ray binary, GX 301–2, as an asymmetric iron $K_\alpha$ line (Watanabe et al. 2003). A detailed spectral analysis of GX 301–2 indicated that the shape of the Compton shoulder depends largely on the absorption column density (which contributes to the number of scatterings) and the consequent smearing with the increase in the electron temperature. Several studies have investigated the dependence of the Compton shoulder on spatial and temporal parameters by assuming different geometries for the reflectors through detailed Monte Carlo simulations (see e.g. Odaka et al. 2011, 2016). Such simulations can be best compared with X-ray spectra acquired with a very high spectral resolution, such as those obtained with micro-calorimeters and broad-band spectroscopy (necessary to assume a proper spectral slope for the illuminating spectrum). Using the current *Chandra* data for OAO 1657 – 415, which are comparatively dimmer (count rate $\sim$ 1/10 of GX 301–2, when compared with the light-curves obtained by Watanabe et al. 2003), we have limited scope to perform such detailed simulations and therefore leave such estimates to further studies.

In the subsequent paragraphs, we will discuss the physical interpretations arising from the presence of the iron emission lines.

### 4.1 Relative fluxes of emission lines

(i) The flux of the Compton shoulder is about 25 per cent (14 per cent and 33 per cent respectively in the HETG and ACIS-S spectra) of the $K_\alpha$ keV line

(ii) $K_\beta$ and $K_\alpha$ of Fe: The ratio of $K_\beta$ to $K_\alpha$ line fluxes ($\eta$) is about 0.20 $\pm$ 0.03 (0.13 $\pm$ 0.04 and 0.28 $\pm$ 0.02 respectively in the HETG and ACIS-S spectra). The expected value of this flux ratio (theoretically) for neutral gas Fe atoms is $\eta = 0.125$ (Kaastra & Mewe 1993), while experimental results for solid Fe give $\eta = 0.1307$ (Pawłowski et al. 2002).

(iii) Fe XXVI (6.97 keV) and Fe XXV (6.7 keV) of Fe: For iron to produce fluorescent lines at 6.4 keV, the ionization parameter is required to be $\xi(= L/nr^2) \leq 10^2$ (Kallman & McCray 1982). In the present case, the ratio of the flux of Fe XXVI (6.97 keV) to Fe XXV (6.7 keV) $\sim 1.76^{-0.01}_{+0.12}$ (from the HETG spectrum), which corresponds to $\xi \geq 10^{3.5}$ (cf. fig. 8 of Ebisawa et al. 1996). Such a high degree of the ionization parameter as well as the presence of Fe XXV and Fe XXVI suggest that the 6.4-keV iron lines in OAO 1657 – 415 are produced in a region significantly farther away from the neutron star, while the the He-like and H-like lines are produced from a different region, nearer to the neutron star.

(iv) $K_\alpha$ of Ni and Fe: The ratio of intensities of $K_\alpha$ of Ni to Fe (from ACIS-S data) is $\sim$0.049 $\pm$ 0.014, consistent with solar abundances (Molendi, Bianchi & Matt 2003). Finally, the possible iron K-absorption edge at $\sim$7.1 keV seen in the X-ray spectrum is consistent with the large absorption column densities.

### 4.2 Size of the 6.4-keV line region

In addition to the highly ionized lines of Fe discussed earlier, the neutral $K_\alpha$ line of iron is also very strong, with an equivalent width of more than 1 keV. An approximate calculation as follows gives us an estimate of the minimum size of the clump and an estimate of the radius at which the iron lines of varying ionization are formed.

We assume that the very high absorption column density and the line equivalent width are the result of the neutron star passing through a dense clump. The hardness ratio does not change significantly during the observation (of $\sim$50 ks), making the minimum size of the clump ($d$) $\sim 5 \times 10^{12}$ cm (assuming a nominal characteristic velocity of the stellar wind of 1000 km s$^{-1}$; Bozzo et al. 2016). Assuming that the clump is spherical and that the neutron star passes through its centre, the absorption is caused by matter along the radius ($d$/2), and the maximum number density ($n$) of the clump

can be estimated as $N_H/0.5d = (0.7\times 10^{24}/2.5 \times 10^{12}) \sim 2.8 \times 10^{11}$ cm$^{-3}$.

Therefore, for an absorbed luminosity (1–10 keV) $L$ of $\sim 1.5 \times 10^{35}$ and required ionization parameter $\xi = L/nr^2 \leq 10^2$, the limiting inner radius for the 6.4-keV line-producing region is ∼2.5 light-seconds. The 6.4-keV line is produced from a region outside this radius, while the H-like and He-like lines are produced from a region very close to the neutron star. One other HMXB in which very distinct regions for different iron emission lines have been ascertained is Cen X–3 (Naik et al. 2011). The H-like and He-like iron emission lines in Cen X–3 are produced in a region larger than the companion star, while the $K_\alpha$ line is produced closer to the neutron star, perhaps in the outer accretion disc (Iaria et al. 2005). For OAO 1657 – 415, we should note that because the region below 2.5 light-seconds is dominated by the ionized H-like and He-like lines, we could in principle also expect a Compton shoulder for these lines. In this case, however, the 6.7- and 6.97-keV lines are too weak for any potential shoulder to be detected the same in the *Chandra* spectrum.

## 5 CONCLUSION

Through a detailed spectral fitting of the ACIS-S and first-order HETG spectra, we report, for the first time, the detection of a Compton shoulder in OAO 1657 – 415, making it only the second X-ray binary in which this feature has been detected. We report a large absorption column density in the X-ray spectrum and that the iron $K_\alpha$ line has a large equivalent width of ∼1 keV. In addition, we report the detection of He-like and H-like lines of iron at 6.7 and 6.97 keV for the first time for this source. From a timing analysis, we report the non-detection of pulsations (with a pulse fraction lower than 2 per cent), perhaps because the neutron star is in a dense environment, leading to many scatterings and a subsequent loss of coherence. Finally, we put a lower limit on the emission line region of the iron $K_\alpha$ line at a distance greater than 2.5 light-seconds from the neutron star.

## ACKNOWLEDGEMENTS

The authors would like to thank the reviewer for his contributions to the paper in the form of useful comments and suggestions. This research has made use of data and software provided by the High Energy Astrophysics Science Archive Research Center (HEASARC), which is a service of the Astrophysics Science Division at NASA/GSFC and the High Energy Astrophysics Division of the Smithsonian Astrophysical Observatory. This research has also made use of data obtained from the Chandra Data Archive and the software provided by the Chandra X-ray Center (CXC) in the application packages CIAO. PP would like to thank Tanmoy Chattopadhyay for useful discussions during the preparation of the manuscript.

## REFERENCES

Anders E., Grevesse N., 1989, Geochim. Cosmochim. Acta, 53, 197
Audley M. D., Nagase F., Mitsuda K., Angelini L., Kelley R. L., 2006, MNRAS, 367, 1147
Barnstedt J. et al., 2008, A&A, 486, 293
Barragán L., Wilms J., Pottschmidt K., Nowak M. A., Kreykenbohm I., Walter R., Tomsick J. A., 2009, A&A, 508, 1275
Bildsten L. et al., 1997, ApJS, 113, 367
Bozzo E., Oskinova L., Feldmeier A., Falanga M., 2016, A&A, 589, A102
Canizares C. R. et al., 2005, PASP, 117, 1144
Chakrabarty D. et al., 1993, ApJ, 403, L33
Chakrabarty D. et al., 1997, ApJ, 474, 414
Chakrabarty D., Wang Z., Juett A. M., Lee J. C., Roche P., 2002, ApJ, 573, 789
Ebisawa K., Day C. S., Kallman T. R., Nagase F., Kotani T., Kawashima K., Kitamoto S., Woo J. W., 1996, Publ. Astron. Soc. Japan, 48, 425
Falanga M., Bozzo E., Lutovinov A., Bonnet-Bidaud J. M., Fetisova Y., Puls J., 2015, A&A, 577, A130
Garmire G. P., Bautz M. W., Ford P. G., Nousek J. A., Ricker G. R., , Jr, 2003, in Truemper J. E., Tananbaum H. D., eds, Proc. SPIE Vol. 4851, X-Ray and Gamma-Ray Telescopes and Instruments for Astronomy, SPIE, Bellingham. p. 28
Iaria R., Di Salvo T., Robba N. R., Burderi L., Lavagetto G., Riggio A., 2005, ApJ, 634, L161
Islam N., Paul B., 2014, MNRAS, 441, 2539
Jenke P. A., Finger M. H., Wilson-Hodge C. A., Camero-Arranz A., 2012, ApJ, 759, 124
Kaastra J. S., Mewe R., 1993, A&AS, 97, 443
Kallman T. R., McCray R., 1982, ApJS, 50, 263
Mason A. B., Clark J. S., Norton A. J., Negueruela I., Roche P., 2009, A&A, 505, 281
Molendi S., Bianchi S., Matt G., 2003, MNRAS, 343, L1
Naik S., Paul B., Ali Z., 2011, ApJ, 737, 79
Odaka H., Aharonian F., Watanabe S., Tanaka Y., Khangulyan D., Takahashi T., 2011, ApJ, 740, 103
Odaka H., Yoneda H., Takahashi T., Fabian A., 2016, MNRAS, 462, 2366
Orlandini M., dal Fiume D., del Sordo S., Frontera F., Parmar A. N., Santangelo A., Segreto A., 1999, A&A, 349, L9
Özbey Arabacı M. et al., 2015, A&A, 582, A53
Paerels F., Cottam J., Sako M., Liedahl D. A., Brinkman A. C., van der Meer R. L. J., Kaastra J. S., Predehl P., 2000, ApJ, 533, L135
Paul B., Nagase F., Endo T., Dotani T., Yokogawa J., Nishiuchi M., 2002, ApJ, 579, 411
Pawłowski F., Polasik M., Raj S., Padhi H. C., Basa D. K., 2002, Nucl. Instruments Methods, Phys. Res. B, 195, 367
Polidan R. S., Pollard G. S. G., Sanford P. W., Locke M. C., 1978, Nature, 275, 296
Pradhan P., Maitra C., Paul B., Islam N., Paul B. C., 2014, MNRAS, 442, 2691
Smith D. A., Takeshima T., 1998, Astron. Teleg., 36
Watanabe S. et al., 2003, ApJ, 597, L37
Watanabe S. et al., 2006, ApJ, 651, 421
White N. E., Pravdo S. H., 1979, ApJ, 233, L121
Wojdowski P. S., Liedahl D. A., Sako M., Kahn S. M., Paerels F., 2004, ApJ, 607, 1071

This paper has been typeset from a TEX/LATEX file prepared by the author.